Prediction of continuous cooling transformation diagram for weld heat affected zone by machine learning

Satoshi Minamoto, Susumu Tsukamoto, Tadashi Kasuya, Makoto Watanabe & Masahiko Demura

Published online: 13 Oct 2022.

Submit your article to this journal ⍐

Article views: 260

View related articles ⍐

View Crossmark data ⍐

Taylor & Francis
Taylor & Francis Group

Prediction of continuous cooling transformation diagram for weld heat affected zone by machine learning

Satoshi Minamoto [a], Susumu Tsukamoto [a], Tadashi Kasuya [b], Makoto Watanabe [c] and Masahiko Demura [a]

aResearch and Services Division of Materials Data and Integrated System, National Institute for Materials Science, Ibaraki, Japan; bDepartment of Materials Engineering, School of Engineering, The University of Tokyo, Tokyo, Japan; cResearch Center for Structural Materials, National Institute for Materials Science, Ibaraki, Japan

ABSTRACT

The continuous cooling transformation (CCT) diagram of steels is very important in considering the phase transformation depending on the cooling rate of a material; however, it is difficult to obtain the diagram for each steel because of much experimental effort required. Therefore, it is important to establish a technique to predict the CCT diagram with good accuracy under arbitrary conditions such as composition and cooling rate. We have developed a prediction model of a CCT diagram for the weld heat affected zone (HAZ) using machine learning based on existing experimental data. The prediction accuracy was improved by separately considering critical cooling rate and temperature at which the transformation starts at various cooling rates, and by using double cross-validation (DCV) to effectively use a small amount of data.
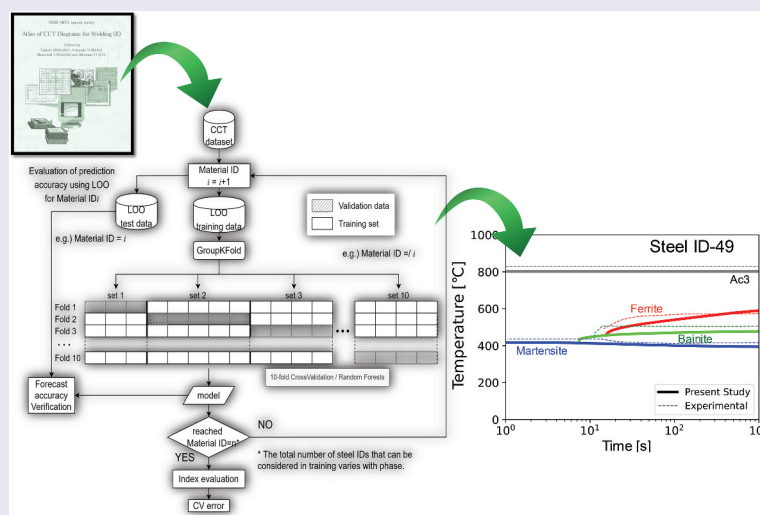
1. Introduction

To evaluate the performance of structural steels, understanding its microstructure after processing is crucial. The continuous cooling transformation (CCT) diagram of a steel plays an important role in providing information on the steel microstructure, as the information includes the start temperatures of phase transformation during cooling, as well as hardness. Since the actual CCT diagram varies significantly with material composition, the CCT diagram has to be constructed for each steel on the basis of experimental results. However, organizing the CCT information obtained for a specific steel is a highly experimental and time-consuming process, and it is difficult to immediately increase the amount of information.

For the prediction of a CCT diagram, there are several models for the transformation of the austenite phase during cooling. The commercial code JMatPro [1], which implements the Kirkaldy–Venugopalan model [2–5] assuming the additivity of time temperature transformation (TTT) diagram, is widely used. A model, that is an improved version of the Johnson–Mehl–Avrami–Kolmogorov (JMAK) model [6–8] has also been reported.

Sci. Technol. Adv. Mater. Meth. 2 (2022) 403

S. MINAMOTO et al.

It has been shown that the CCT diagrams constructed using the addition rule can give erroneous estimates [9,10]. In addition to the refinement of transformation modeling, recent developments in data science have led to the prediction of transformation using machine learning and deep learning, as shown in Table 2. However, the number of reports that can show the overall CCT diagram is still limited because the prediction of Ac_3 temperature and the phase transformation start temperatures of ferrite (F), bainite (B), pearlite (P), and martensite (M) phases are evaluated separately using different data.

Trzaska has developed a linear regression formula [12], but it is not applicable to CG HAZ, the prediction models developed by Geng et al. are limited to Ni–Cr–Mo steels [16] and low alloy steels [17]. However, they do not predict the Ac_3 and critical cooling rate, which are essential for constructing the CCT diagrams for unknown materials as mentioned in the last paragraph of section 2.3. Miettinen et al. [21] used the critical cooling rate, which is expected to improve the accuracy in the prediction of a CCT diagram, but separate determination of intergranular components is required.

The toughness of a weld joint often deteriorates in the vicinity of the coarse-grained heat affected zone (CG HAZ), where the prior austenite grain size is the largest. For this reason, many CCT diagrams for welding have been developed for the CG HAZ, where the maximum temperature is between 1350°C and 1400°C. For example, CCT diagrams of structural steels for welding from Japan Iron and Steel Institute [22], NRIM CCT Atlas 1,2 [23–25] published by NRIM (now National Institute for Materials Science (NIMS)), and CCT diagrams for duplex stainless steels [26] are available. These CCT data must be useful for developing prediction models of CCT diagrams for CG HAZ.

On the other hand, with the progress of computational science and meso- and macro-scale computational techniques such as the CALPHAD (CALculation of PHAse Diagrams) method, the phase field method, and the finite element method, it has become common to consider the performance of structural materials according to the PSPP model (process, structure, property, and performance) [27]. It is now considered effective to consider the performance of materials. In Japanese SIP-MI projects [28,29], a number of workflows have been developed to consistently predict the material performance of weld HAZ on the basis of the PSPP concept [30–38]. Information on the microstructure of a material is crucial for the accurate material performance prediction using such workflows. To predict the microstructure of the weld HAZ, we have constructed a prediction model of the CCT diagram of an arbitrary composition from using experimental data by machine learning.
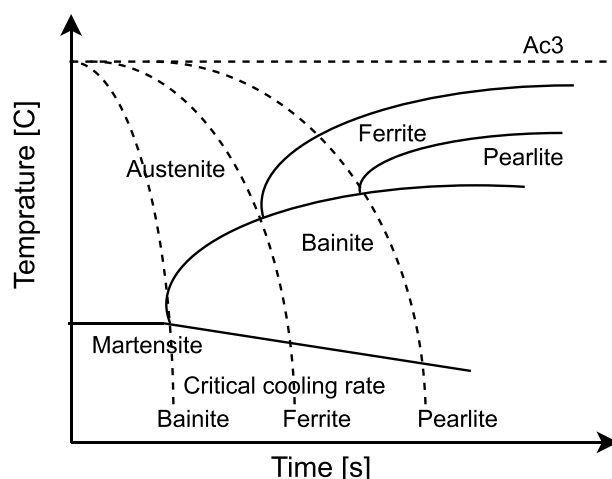

Figure 1. Schematic illustration of continuous cooling transformation (CCT) diagram for steel.

2. Building a prediction model of CCT diagram for weld HAZ

2.1. CCT diagram of steel and the thermophysical properties required for predicting the diagram

A schematic illustration of the CCT diagram is shown in Figure 1, where the horizontal axis is the time elapsed from the Ac_3 temperature during cooling and the vertical axis is the temperature. The solid lines in the figure are the transformation start temperatures for the F, P, B, and M and the dashed lines are the critical cooling rates for the F, P, and B, beyond which these phases do not appear. The critical cooling rates, which will be discussed later, are very important for drawing the CCT diagram. In order to predict the CCT diagram for a given composition, it is necessary to predict the following parameters: Ac_3, the critical cooling rates of F, P, and B, and the transformation start temperatures of F, P, B, and M at various cooling rates.

When the cooling rate is low, the transformation proceeds in the order of F, P, and B. In general, as the cooling rate increases, the transformation temperature decreases, the amount of F and P decreases, and the amount of B and M increases, resulting in an increase in hardness.

The procedure to construct a prediction model of a CCT diagram is as follows: (1) digitizing and organizing the CCT data, (2) predicting Ac_3, (3) predicting the critical cooling rate, (4) estimating the time and temperature of phase transformation at several cooling rates, and (5) drawing the comprehensive CCT diagram.

2.2. CCT diagram data: NRIM atlas 1

The CCT diagram depends on not only the composition but also the austenite grain size (austenitization conditions). However, the austenitization conditions often vary in the literature, and mixing all the austenitization conditions as training data may lead to inaccuracy. The CCT
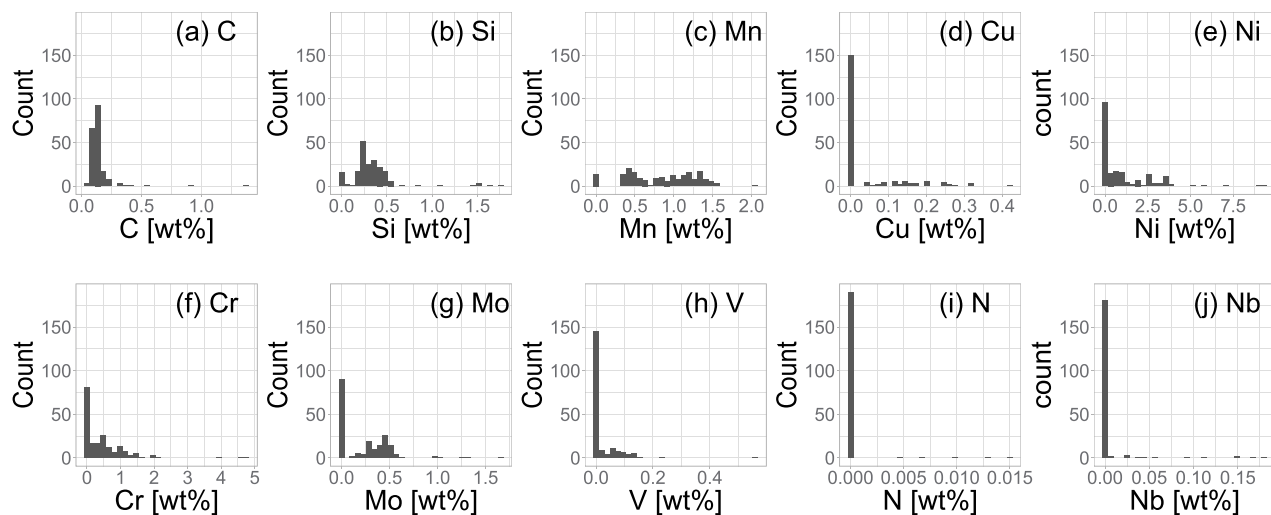
Sci. Technol. Adv. Mater. Meth. 2 (2022) 404

S. MINAMOTO et al.

Figure 2. Histograms of elemental amounts listed in NRIM Atlas 1, (a) C, (b) Si, (c) Mn, (d) Cu, (e) Ni, (f) Cr, (g) Mo, (h) V, (i) N, (j) Nb.

diagram data NRIM Atlas 1 [23,24] is intended for evaluating the microstructure of CG HAZ and contains 195 CCT diagrams for various types of steels, as shown in Table 3. All diagrams are created under the same austenitization conditions (peak temperature: 1350°C, holding time: 0 sec). Then, we used these 195 CCT diagrams as the training data to create the model for predicting the CCT diagram. The NRIM Atlas 1 data are also available on NIMS MatNavi [39].

Histograms of the chemical composition of the steels in NRIM Atlas 1 are shown in Figure 2. Nitrogen (N) has not been measured in some steels and is treated as zero if not stated. As a result, about 150 steels have a nitrogen content of zero. The mean and standard deviation of the alloy compositions are shown in Table 4. All information on alloy composition is given in Table 1.

First, CCT diagrams stored as printed data were scanned with high accuracy and stored as electronic data using a general-purpose digitizer. The obtained electronic data were used to create an approximate curve for the phase transformation start line of each steel. In the case of data not available owing to low cooling rate, the data were supplemented by transformation in which the transformation line was approximated by a monotonically increasing function. The validity of the CCT datasets was confirmed by comparing the obtained data with micrographs and so on.

Table 1. Techniques used to predict transition temperature in previous studies.

Predicted temperature	Method
Ac_3	ANN [11], LR [12,13]
Martensite start	ANN [11,14,15], kNN [16,17], LR [12,13,18]
Ferrite start	LR [18,19], RF [16,17]
Pearlite start	LR [18]
Bainite start	ANN [11,18,20], LR [12,19], RF [16,17]

ANN: Artificial Neural Network.
CNN: Convolutional Neural Network.
kNN: *k*-nearest neighbors.
LR: Linear Regression.
RF: Random Forests.

Table 2. Steel grades listed in NRIM Atlas 1.

Types of steel	Number
Simple Fe–C–X Alloy (X:Si,Ni,Cr,Cu,Mo,Ti, V, Nb, Al, B)	35
HT-400 MPa class	3
HT-490 MPa class	21
HT-590 MPa class	33
HT-690 MPa class	29
HT-780 MPa class	28
HT-880 MPa class	12
HT-980 MPa class	7
Ultra high tensile strength steel	6
Pressure vessel steel	2
Line-pipe steel	2
Low temperature steel	5
Heat resistance low alloy steel	12

Table 3. Mean and standard deviation of alloy compositions in wt%.

Element	Mean	Standard deviation
C	0.149	0.119
Si	0.340	0.266
Mn	0.837	0.432
Cu	0.039	0.082
Ni	0.978	1.540
Cr	0.458	0.687
Mo	0.236	0.272
V	0.021	0.055
N	0.00025	0.00167
Nb	0.00555	0.02580

Table 4. Coefficient of determination (R^2), and the root mean square error (RMSE), and the mean absolute error (MAE) for Ac_3 temperature predictions using the NRIM Atlas 1 data.

Model for Ac_3	R^2	RMSE [°C]	MAE [°C]
Present study	0.661	27.0	21.2
Trzaska [12]	0.391	44.9	36.0
Kim [13]	0.469	34.4	27.8
Andrews [40]	0.332	48.6	39.1

Sci. Technol. Adv. Mater. Meth. 2 (2022) 405

S. MINAMOTO et al.

Some CCT diagrams were excluded from 195 datasets. The effect of boron (B) is very large and should be included as a descriptor for prediction because of its possible effect of shifting the CCT line to the longer side; however, the insufficient description of the amount of B in NRIM Atlas 1 makes it difficult to evaluate its effect. Therefore, it was decided to exclude B from the explanatory variables and B-containing steels (15 steels) from the training data in the present study. We will discuss the effect of B in the next paper. Three steels with a high C content of 0.5 wt% or more have been excluded, due to the different transformation processes. Formation of some precipitates may affect the CCT diagram, because the CCT curves are determined by the solute content of each element just before the transformation. However, we consider the effect of precipitates is included in the non-linear model of the present study. Only four steels with a Nb content of 0.14 wt% or more have been excluded, because the content is too high compared with the commercial steels. In addition, questionable datasets were excluded (9 steels); then, dataset for 164 steels was used.

2.3. Machine learning algorithms and descriptor selection

Four machine learning algorithms, i.e. random forests [41], multiple regression, XGBoost, and support vector regression methods, have been tested and found that the random forests provided the best prediction performance. Thus, we used the random forests for the subsequent analysis. The random forests is an ensemble learning algorithm with decision trees as weak learners. The data were sampled to ensure that the data of the same steel grade are not included in both the training and test datasets at the same time (GroupKFold sampling). The hyperparameter of the random forests is the ratio of the descriptors used in each branch. Hyperparameters are optimized using a combination of grid search and Bayesian optimization techniques to select the best model.

In general, performing cross-validation (CV) by dividing the data into training and validation data when the size of the available dataset is small will result in a large variation in the accuracy of the machine learning model depending on the sampling method [42]. To maximize the use of data on a small number of steels, we decided to use double cross validation (DCV) [43], which is a double nested structure of CVs. For the outer CV, we adopt the leave-one-out (LOO) method, where only one dataset is left for testing and the rest is used for training, to evaluate the generalization performance. In the inner CV, the data set with one point removed by LOO is used for 10-fold cross-validation to adjust the hyperparameters. The final prediction model is built by adjusting the hyperparameters using all the data. The R and Python languages were used for the analysis. The random forests function

was implemented in the R library, and the LOO and data processing parts were implemented in R. The part related to drawing was implemented in Python. Since all the data are used as training data, it is difficult to evaluate the generalization performance. However, we believe that the results of repeated evaluations by excluding a single point in LOO are close to the prediction results obtained by treating all the data as unknown data. The flowchart for DCV is shown in Figure 3. When the number of data is small, there is a problem of large variation of model performance due to random sampling using general k-fold CV. However, when DCV is used, variation is minimized because all data can be used for model building. The coefficient of determination R^2 is evaluated by solving Eq. (1).

$$R^2 = \frac{\sum_i \left(y_i^{obs} - y_i^{pred}\right)^2}{\sum_i \left(y_i^{obs} - \overline{y^{obs}}\right)^2}, \qquad (1)$$

where y_i^{obs} and y_i^{pred} are the observed and predicted values for ith data, respectively, and the overline denotes the average of the values.

According to the experimental conditions of the NRIM CCT Atlas 1 [23], the data supervised in this study, the Ac_3 measurement is considered to be approximately equal to A_3 because the sample was heated slowly. In the CCT diagram measurements, the specimens were rapidly heated to 1350°C and immediately cooled. The cooling is given a thermal cycle similar to the temperature history measured at the heat affected zone during welding. The old austenite grain size was found to be about 100 . Figure 4 shows the procedure for predicting the CCT diagram. Using the alloy composition and the logarithmically transformed cooling rate as descriptors, we first predict the Ac_3 temperature, and the predicted temperature is used. Next, the critical cooling rates of F, P and B were predicted to determine the upper limit of the cooling rate for the transformation of each phase. The transformation start time was predicted between 1 and 1000 sec. The critical cooling rate was used to determine the presence of phase transformation. Then we added the cooling rate as a descriptor, and the transformation start temperatures and times for F, P, and B were predicted for 40 equally spaced cooling curves on a logarithmic scale, in the range below the critical cooling rate for each phase. For M, the transformation start temperature was predicted for all cooling rates. The prediction of the transformation start time near the nose has a larger prediction error owing to the smaller curvature of the CCT line. Therefore, the CCT curve at the tip of the nose was represented by connecting the intersection of the critical cooling rate line and the transformation start temperature line learned on the long side with a B-spline curve [44].

Figure 5(a) shows a two-dimensional histogram of all the data plotted for the ferrite phase used in this
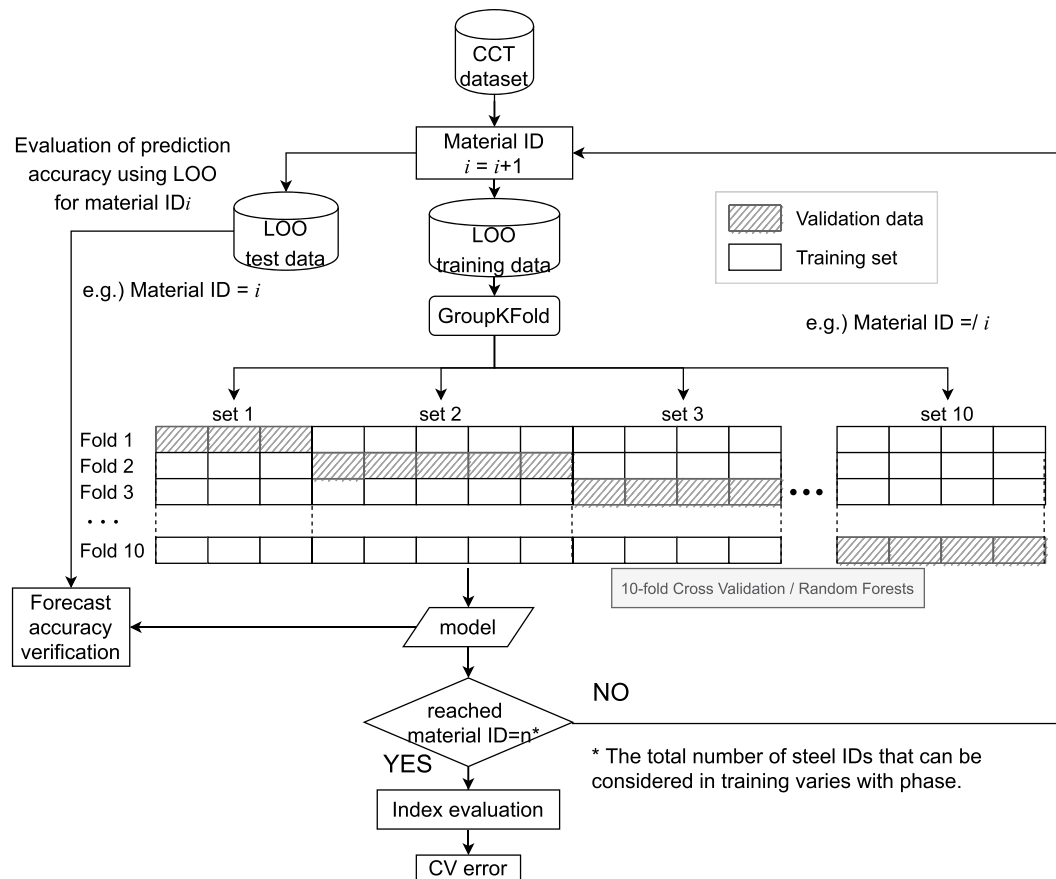
Figure 3. Flowchart of DCV and construction of final model.
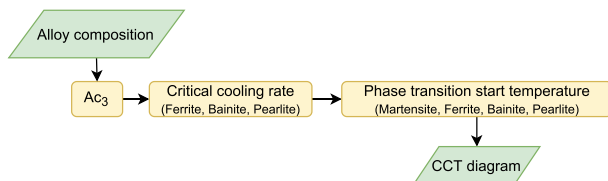
Figure 4. Procedure for predicting CCT diagram.

study, where the number of data points used for training is small in the high cooling rate and low-temperature region as shown in the red circle. In addition, only the transformation start data of low hardenable steels are available in this region. If the ferrite transformation temperature of high hardenable steel is predicted under such a condition, inaccurate

(a) 2-D histogram of experimental data used for the prediction of ferrite phase (3735 points).

(b) (Solid line) Prediction lines truncated at critical cooling rate for each phase, (broken line) Predictions based on only start temperature, (Ac$_3$ (black), M (blue), F (red), B (green), P (yellow)).

Figure 5. (A) Variation in the number of data in temperature-time space, and (b) difference between prediction lines with and without considering of critical cooling rate.

prediction results are obtained in high cooling rate region as shown in the dotted line in Figure 5(b). Thus, it is very important to include an index to distinguish the presence of transformation by separately predicting the critical cooling rate.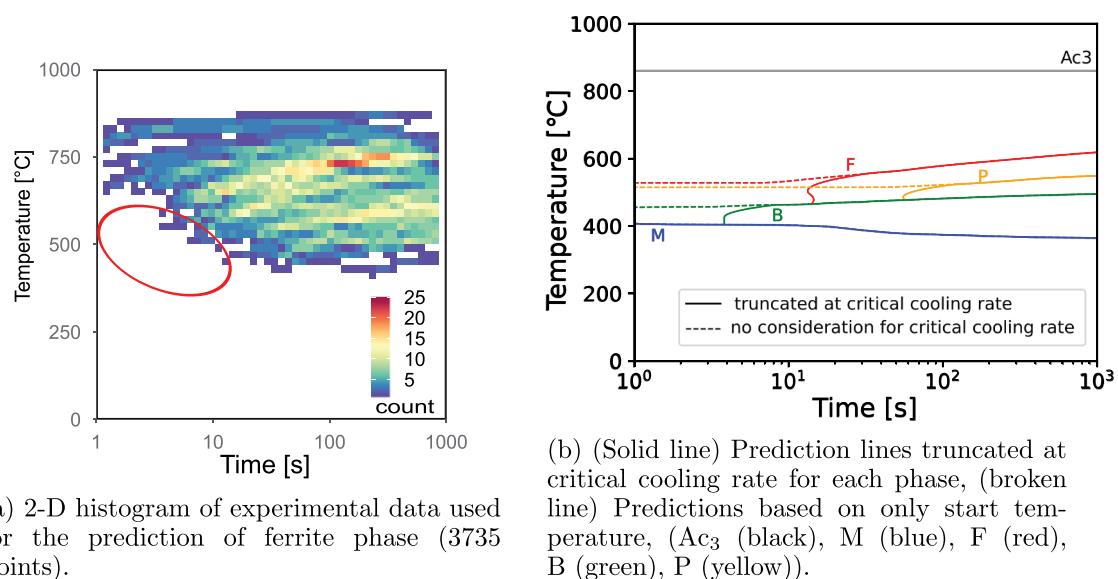 Therefore, as shown in Figure 5(b), the nose position of the transformation was determined by the critical cooling rate, and the prediction line of the transformation temperature was truncated above the critical cooling rate.

3. Results and discussion

3.1. Performance evaluation

A comparison between the predicted results and the experimental data for Ac_3 temperature is shown in Figure 6 and the performance evaluation is shown in Table 5., where R^2 is the coefficient of determination, RMSE is the root mean square error, and MAE is the mean absolute error. Table 5 also includes the
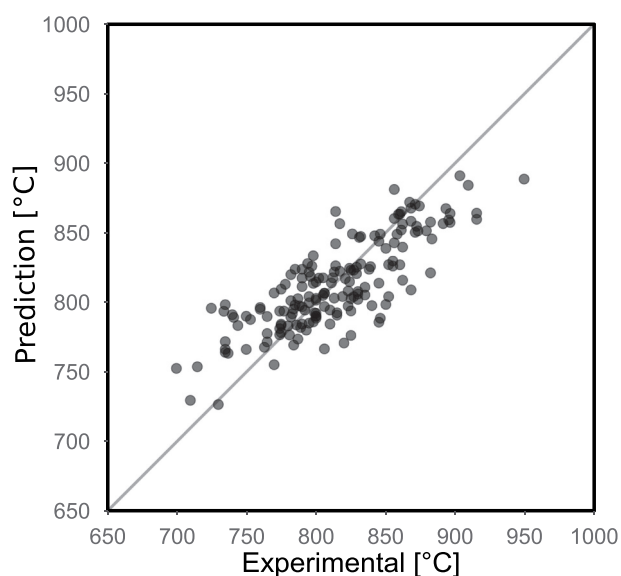

Figure 6. Prediction of Ac_3 temperatures.

Table 5. Coefficient of determination (R^2), the root mean square error (RMSE), and the mean absolute error (MAE) for Ms temperature (martensite phase transition start temperature).

Model for Ms	R^2	RMSE [°C]	MAE [°C]
Present study	0.566	20.1	15.9
Trzaska [12]	0.477	25.9	19.9
Kim [13]	0.551	20.8	16.4
Capdevila [14]	0.505	29.8	24.9
Andrews [40]	0.462	27.9	21.1

parameters evaluated in some references, where all Ac_3 data used in this study were predicted using the formulas [12,40] or machine learning model [13].

By comparing the prediction performance in this study with those in other references, we can see that the prediction accuracy in this study is higher than those in other references.

In all references, the Ms temperature was predicted when martensite was completely formed. In this study, however, performance in the region of constant Ms temperature with respect to time was also evaluated.

The results of the DCV method for the prediction of the critical cooling rates of (a) ferrite, (b) pearlite, and (c) bainite are shown in Figure 7. The performance of the training model for predicting the critical cooling rate for using unknown data is shown in Table 6. The accuracy of the prediction of the critical cooling rate for pearlite is slightly lower than that for the other phases. This might be due to the small number of data for pearlite and the fact that the accuracy of the experimental data is lower than that for the other phases, because it is difficult to detect the pearlite transformation only by dilatation measurement.

The data obtained in this study for the prediction of the start temperature of transformation for several cooling rates are shown in Figure 8. The prediction points for the same steel are presented continuously for different cooling rates. The performance of this prediction model for the transformation temperature is shown in Table 7, and we found that each start temperature was predicted with good accuracy of undefined ±30°C.

3.2. Evaluation of predicted CCT diagrams

A prediction model of the CCT diagram, constructed using the random forests method with double CV, was used to compare the CCT diagram calculated using the actual steel composition with the experimental results. In the evaluation, a prediction model was built by deleting one of the steels concerned. Several types of steel were selected according to their proof stress and their prediction results were compared with experimental results. ID-49 (SM50B), which is equivalent to SM490, was selected for the 490 MPa grade, ID-137 for the 590 MPa grade and ID-48 and 130 for the 780 MPa grade. The composition of each steel is shown in Table A1 in section Appendix A.

Table 6. Coefficient of determination (R^2) and the root mean square error (RMSE), the mean absolute error (MAE) for the model for critical cooling rate for various phases.

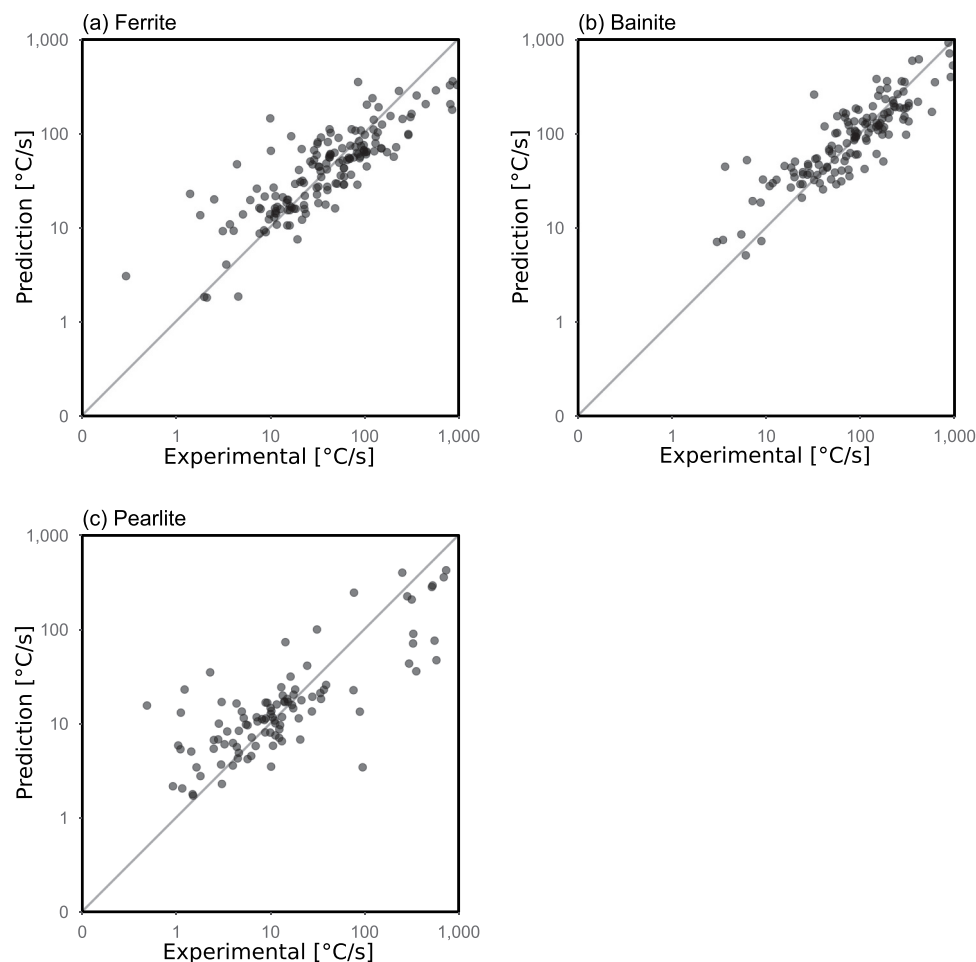| Phase	R^2	RMSE [log(°C/sec)]	MAE [log(°C/sec)]
Ferrite	0.688	0.335	0.251
Pearlite	0.638	0.460	0.330
Bainite	0.826	0.277	0.223

Figure 7. Prediction and verification results of critical cooling rate for various phases. ((a) F, (b) B, and (c) P).

Table 7. Coefficient of determination (R^2), the root mean square error (RMSE), and the mean absolute error (MAE) for phase transition start points.

Phase	R^2	RMSE [°C]	MAE [°C]
Martensite	0.483	26.4	20.3
Ferrite	0.876	34.2	27.4
Bainite	0.507	30.3	23.6
Pearlite	0.592	35.4	27.5

Figure 9 shows the prediction results for each steel. The prediction model is generated by excluding the relevant steel and predicted the eligible steel. Good agreements of prediction results with the experimental results are obtained for each steel. When the LOO approach is used to evaluate the prediction performance for unknown data, a prediction model is built without the data concerned. However, in the end, the data for all steels were included in the prediction model, which meant that the model has also been adjusted for selected steels. Furthermore, the prediction performance is also expected to improve the prediction accuracy in the vicinity of the steel compositions.

When compared to other reports, it is difficult to evaluate the performance indicators alone because of the different steel grades handled and the variability in the number of data. Therefore, to evaluate the constructed model performance, results from this study were compared to JMatPro, which is a universally constructed and widely used model.

All CCT diagrams used in the present study were also predicted using JMatPro, assuming an austenitization temperature of 1350°C. The prior austenite grain size was set to 100 , which was the same assumption our prediction was based on as mentioned in section 2.3. Then data conversion was carried out for the results obtained, using the Ac_3 temperature of each steel as the reference for the cooling start time. As for the fraction of the formed phases, since the experimental values in NRIM Atlas 1 were obtained with a standard of 1%, the same standard was used in the JMatPro calculation. Figure 10 shows one example where the CCT diagram of ID-48 steel was predicted. Figure 9(c) shows good prediction accuracy, whereas F and B are shifted to the long time side in JMatPro, and the temperature for prediction tends to be high. Figure 11 shows the two-dimensional histograms of ferrite transformation start temperature in NRIM Atlas 1 (experimental), predicted in this study and using JMatPro for all steels. It can be seen that the overall prediction of the transformation start time derived from JMatPro shifts to the longer time side and higher temperatures.
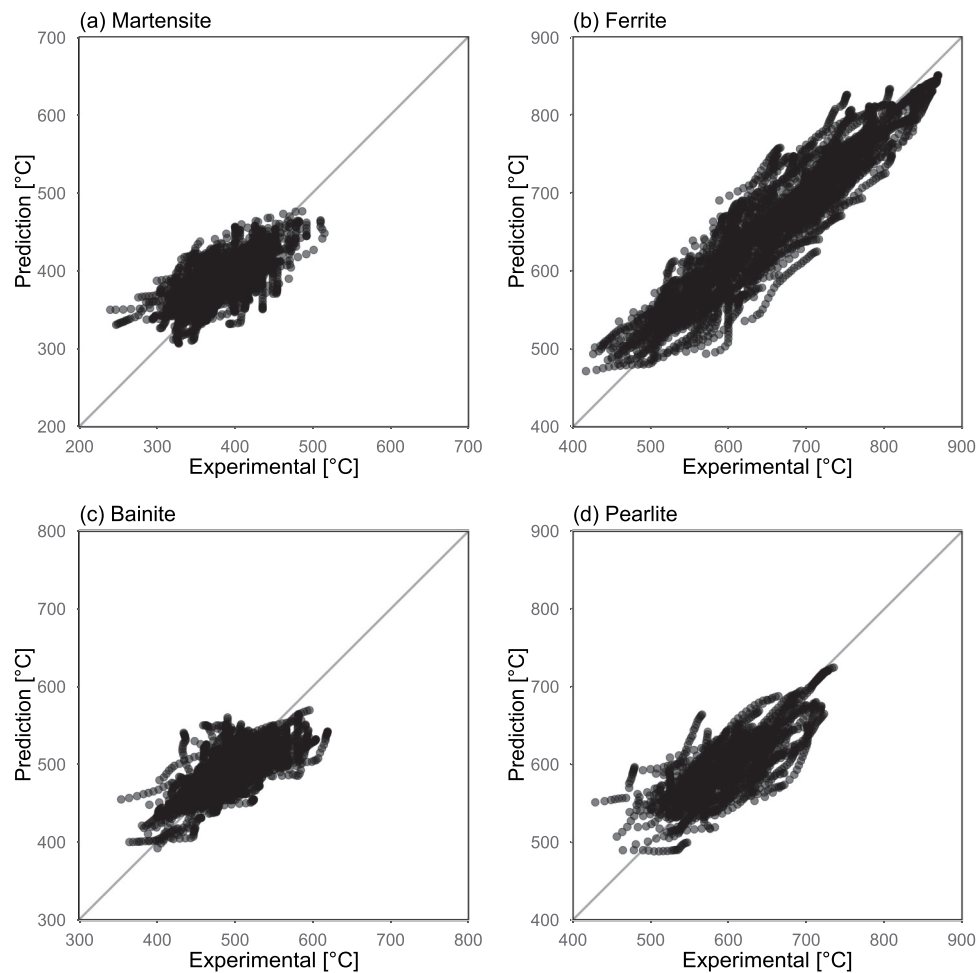
Figure 8. Prediction and verification results of transformation start temperature for various phases: (a) M, (b) F, (c) B, and (d) P.

(a) ID-49 (480 MPa,
Fe–0.140C–0.320Si–1.320Mn–0.003V)

(b) ID-137 (590 MPa,
Fe–0.160C–0.450Si–1.120Mn–0.040Ni–
0.060Cr–0.020Mo–0.011V)

(c) ID-48 (780 MPa,
Fe–0.100C–0.230Si–0.600Mn–2.650Ni–
0.470Cr–0.450Mo)

(d) ID-130 (780 MPa,
Fe–0.140C–0.220Si–1.400Mn–0.760Ni–
0.550Mo)

Figure 9. Evaluated CCT diagrams for the alloys (a) ID-49, (b) 137, (c) 48, (d) 130. M(blue), F(red), B(green), and P(yellow).

Figure 10. CCT diagram evaluated using JMatPro for the alloy of ID-48 for Ac$_3$(black), M(blue), F(red), and B(green).

Figure 11. 2-D histograms of ferrite phase transition start temperature at various cooling rates for all target steels, predicted (a) in present study and (b) using JMatPro.

4. Summary

Although CCT data provide a wealth of information on the cooling rate dependent phase transformation of steels, the amount of available experimental data is not sufficient and is difficul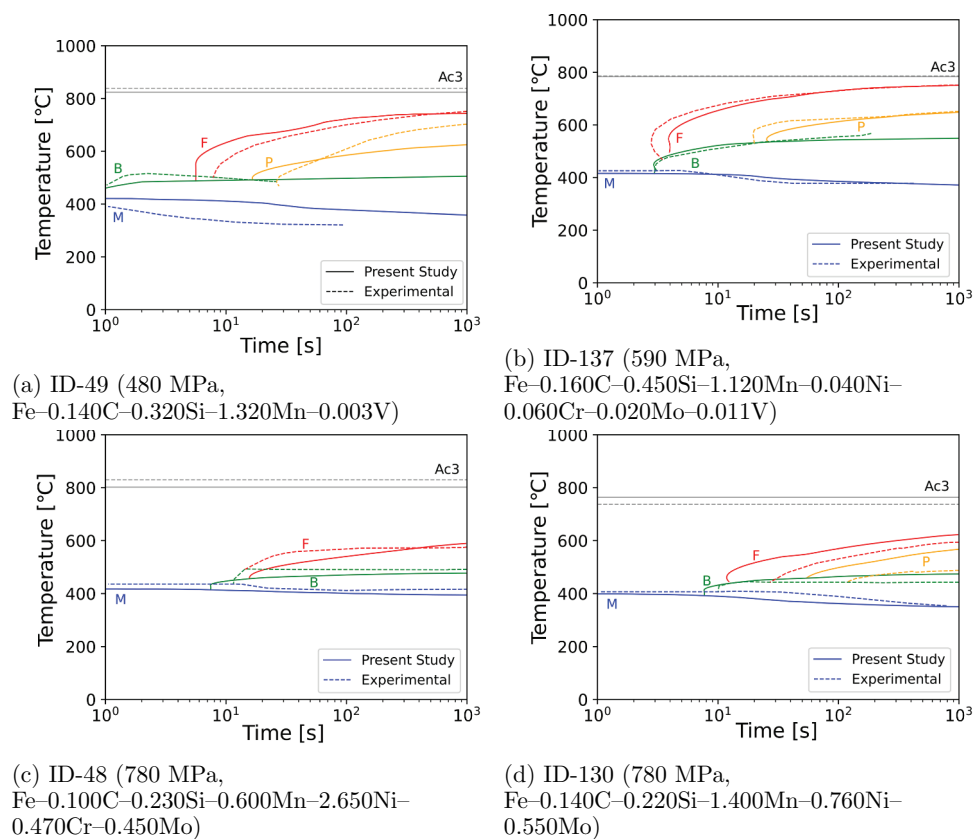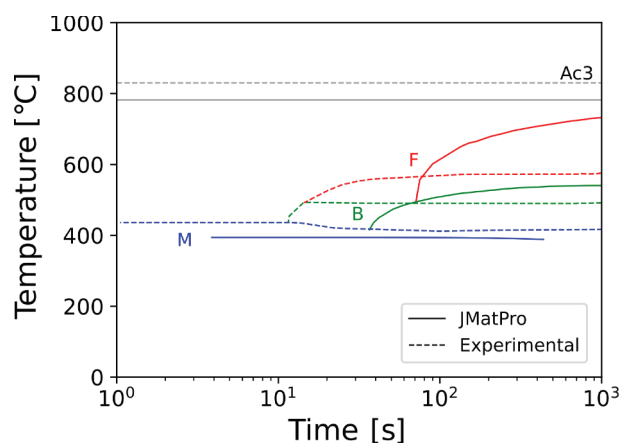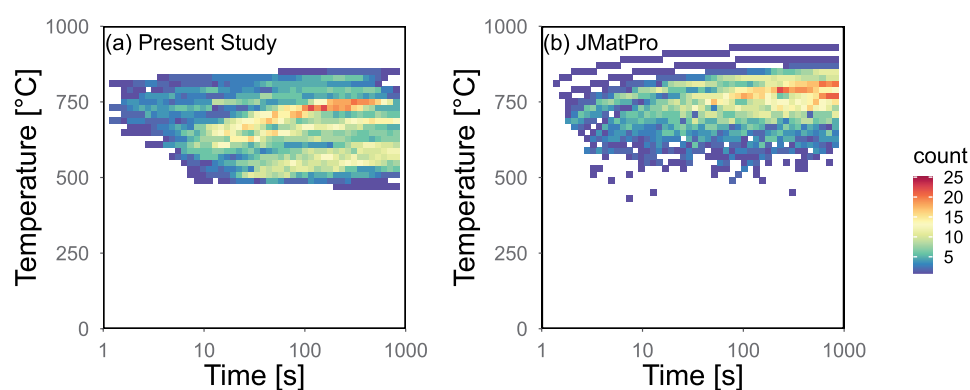t to increase. In the present study, a prediction model for CCT diagrams of weld HAZ was developed using machine learning techniques with existing experimental data on CCT diagrams as training data. The data were carefully extracted from the literature, digitized, and validated with respect to the accuracy of individual data. In constructing the machine learning model, we adopted the method of predicting the transformation start temperature and the critical cooling rate separately, and created the prediction model using the DCV method that maximizes the use of a small number of data. As a result, we were able to construct a prediction model with higher accuracy for a wider range of steel products than in the case of using previous prediction models. The CCT diagram prediction model developed in this study has already been implemented in a system named MInt [28,29] that we have built under the concept of the PSPP model and can be connected to various computational workflows. The model is expected to contribute to the accurate understanding of microstructure information of materials. A hardness prediction model [45] which was developed by one of our authors (T.K.) will be implemented in the future.

Disclosure statement

No potential conflict of interest was reported by the author(s).

ORCID

Satoshi Minamoto iD http://orcid.org/0000-0003-4023-5800

Sci. Technol. Adv. Mater. Meth. 2 (2022) 411

S. MINAMOTO et al.

Susumu Tsukamoto [iD] http://orcid.org/0000-0001-9011-2708

Tadashi Kasuya [iD] http://orcid.org/0000-0002-3303-0770

Makoto Watanabe [iD] http://orcid.org/0000-0002-5064-9583

Masahiko Demura [iD] http://orcid.org/0000-0002-7308-3041

References

[1] Saunders N, Guo UKZ, Li X, et al. Using JMatPro to model materials properties and behavior. JOM. 2003 Dec;55(12):60–65. DOI:10.1007/s11837-003-0013-2

[2] Kirkaldy J, Sharma R. A new phenomenology for steel it and CCT curves. Scr Metall. 1982;16 (10):1193–1198.

[3] Kroupa A, Kirkaldy J. Computed multicomponent phase diagrams for hardenability (H) and HSLA steels with application to the prediction of microstructure and mechanical properties. J Phase Equilib. 1993;14 (2):150–161.

[4] Kirkaldy J, Thomson B. Prediction of multicomponent equilibrium and transformation diagrams for low alloy steels. In: Hardenability concepts with applications to steel. 1977. p. 82–125.

[5] Nakata T, Kasugai T. SH-CCT diagrams for welding and continuous cooling transformation behaviour for ductile cast iron. Int J Cast Met Res. 1997;10 (2):99–103.

[6] Avrami M. Kinetics of phase change. II transformation-time relations for random distribution of nuclei. J Chem Phys. 1940;8(2):212–224.

[7] Pohjonen A, Somani M, Porter D. Modelling of austenite transformation along arbitrary cooling paths. Comput Mater Sci. 2018;150:244–251.

[8] Pohjonen A, Somani M, Porter D. Effects of chemical composition and austenite deformation on the onset of ferrite formation for arbitrary cooling paths. Metals. 2018;8(7). DOI:10.3390/met8070540.

[9] Hawbolt E, Chau B, Brimacombe J. Kinetics of austenite-pearlite transformation in eutectoid carbon steel. Metall Trans A. 1983;14(9):1803–1815.

[10] Zhu Y, Lowe T. Application of, and precautions for the use of, the rule of additivity in phase transformation. Metall Trans B. 2000;31(4):675–682.

[11] Garcia-Mateo C, Capdevila C, Caballero F, et al. Artificial neural network modeling for the prediction of critical transformation temperatures in steels. J Mater Sci. 2007 01;42:5391–5397. DOI:10.1007/s10853-006-0881-2

[12] Trzaska J. Calculation of critical temperatures by empirical formulae. Arch Metall Mater. 2016;61 (2B):981–986.

[13] Kim H, Inoue J, Okada M, et al. Prediction of Ac3 and martensite start temperatures by a data-driven model selection approach. ISIJ Int. 2017;57(12):2229–2236. DOI:10.2355/isijinternational.ISIJINT-2017-212

[14] Capdevila C, Caballero FG, de Andreacutes CG. Determination of Ms temperature in steels: a bayesian neural network model. ISIJ Int. 2002;42 (8):894–902.

[15] Sourmail T, Garcia-Mateo C. A model for predicting the Ms temperatures of steels. Comput Mater Sci. 2005;34(2):213–218.

[16] Geng X, Wang H, Ullah A, et al. Prediction of continuous cooling transformation diagrams for Ni-Cr-Mo welding steels via machine learning approaches. JOM. 2020;72:3926–3934.

[17] Geng X, Mao X, Wu HH, et al. A hybrid machine learning model for predicting continuous cooling transformation diagrams in welding heat-affected zone of low alloy steels. J Mater Sci Tech. 2022;107: 207–215. DOI:10.1016/j.jmst.2021.07.038

[18] Miettinen J, Koskenniska S, Somani M, et al. Optimization of the CCT curves for steels containing Al. Cu B Metall Mater Trans B. 2021 03;52:1640–1663. DOI:10.1007/s11663-021-02130-9

[19] Isasti N, García-Riesco PM, Jorge-Badiola D, et al. Modeling of CCT diagrams and ferrite grain size prediction in low carbon Nb-Mo microalloyed steels. ISIJ Int. 2015;55(9):1963–1972. DOI:10.2355/isijinternational.ISIJINT-2015-036

[20] Hüter C, Yin X, Vo T, et al. A pragmatic dataset augmentation approach for transformation temperature prediction in steels. Comput Mater Sci. 2020;176: 109488. DOI:10.1016/j.commatsci.2019.109488

[21] Miettinen J, Louhenkilpi S, Kytönen H, et al. IDS: thermodynamic–kinetic–empirical tool for modelling of solidification, microstructure and material properties. Math Comput Simul. 2010;80(7):1536–1550. DOI:10.1016/j.matcom.2009.11.002.

[22] The Iron and Steel Institute of Japan, Production Engineering Division. [CCT diagrams of structural steels for welding]. Tokyo: The Iron and Steel Institute of Japan; 1997. Japanese.

[23] Kasugai T, Fujita M Atlas of CCT diagrams for welding.(i). NRIM-special-report No 99-02. 1999. Available from: https://mdr.nims.go.jp/concern/publications/1g05fb663.

[24] Fujita M, Miyamoto K, Okada A, et al. Database on CCT diagrams for welding: presentation and an example of cooperative utilization with other welding information on the internet. J Inf Proc Manag. 2001 01;43:819–831. DOI:10.1241/johokanri.43.819

[25] Ishikawa T, Yurioka N, Yamazaki M, et al. Atlas of CCT diagrams for welding.(ii). NIMS-MITS-special-report. 2008.

[26] Zong Y, Liu C. Continuous cooling transformation diagram, microstructures, and properties of the simulated coarse-grain heat-affected zone in a low-carbon bainite E550 steel. Metals. 2019;9(9). DOI:10.3390/met9090939

[27] Olson G, Kuehmann C. Materials genomics: from CALPHAD to flight. Scr Mater. 2014;70:25–30.

[28] Demura M, Koseki T. SIP-Materials integration projects. Mater Trans. 2020 Nov;61(11):2041–2046.

[29] Minamoto S, Kadohira T, Ito K, et al. Development of the materials integration system for materials design and manufacturing. Mater Trans. 2020;61 (11):2067–2071. DOI:10.2320/matertrans.MT-MA2020002

[30] Enoki M. Development of performance prediction system on SIP-MI project. Mater Trans. 2020;61 (11):2052–2057.

[31] Shibanuma K, Ueda K, Ito H, et al. Model for predicting fatigue life and limit of steels based on micromechanics of small crack growth. Mater Des. 2018;139:269–282.

[32] Tabuchi M, Hongo H, Matsunaga T. Long-Term creep strength and fracture of Gr.91 steel welds. Mater High Temp. 2017;34(5–6):466–472.

[33] Sakurai J, Inoue J, Demura M, et al. Descriptor extraction on inherent creep strength of carbon steels by

Sci. Technol. Adv. Mater. Meth. 2 (2022) 412

S. MINAMOTO et al.

exhaustive search. Int'l Conf Comput Exper Eng Sci. 2019 Jan;22(2):128. DOI:10.1080/27660400.2021.1951505.

[34] Bulgarevich DS, Tsukamoto S, Kasuya T, et al. Automatic steel labeling on certain microstructural constituents with image processing and machine learning tools. Sci Technol Adv Mater. 2019 Dec;20 (1):532–542. DOI:10.1080/14686996.2019.1610668

[35] Kitano H, Tsujii M, Kusano M, et al. Effect of plastic strain on the solidification cracking of hastelloy-X in the selective laser melting process. Addit Manuf. 2021Jan;37:101742.

[36] Izuno H, Demura M, Tabuchi M, et al. Data-Based selection of creep constitutive models for high-Cr heat-resistant steel. Sci Technol Adv Mater. 2020 Jan;21(1):219–228. DOI:10.1080/14686996.2020.1738268

[37] Izuno H, Demura M, Yamazaki M, et al. Damage model determination for predicting creep rupture time of 2 1/4cr-1mo steel weld joints. Mater Trans. 2021;62(7):1013–1022. DOI:10.2320/matertrans.MT-MA2020004

[38] Mototake Y, Izuno H, Nagata K, et al. A universal Bayesian inference framework for complicated creep constitutive equations. Sci Rep. 2020 Dec;10 (1):10437. DOI:10.1038/s41598-020-65945-7

[39] MatNavi NIMS. [cited Jun 2022]. Available from: https://mits.nims.go.jp/

[40] Andrews K. Empirical formulae for the calculation of some transformation temperatures. J Iron Steel Inst. 1965;203:721–727.

[41] Breiman L. Random forests. Mach Learn. 2001;45 (1):5–32.

[42] Cawley GC, Talbot NLC. On over-fitting in model selection and subsequent selection Bias in performance evaluation. J Mach Learn Res. 2010;11 (70):2079–2107. http://jmlr.org/papers/v11/cawley10a.html

[43] Filzmoser P, Liebmann B, Varmuza K. Repeated double cross validation. J Chemom. 2009;23 (4):160–171.

[44] Dierckx P. Algorithms for smoothing data with periodic and parametric splines. Comput Graphics Image Process. 1982;20(2):171–184.

[45] Kasuya T, Inomoto M, Okazaki Y, et al. HAZ hardness prediction of boron-added steels. Weld World. 2021 Apr;65(8):1609–1621. DOI:10.1007/s40194-021-01111-5

Sci. Technol. Adv. Mater. Meth. 2 (2022) 413

S. MINAMOTO et al.

Appendix A

Alloy compositions in NRIM Atlas 1

The alloy compositions in NRIM Atlas 1 are listed in Table A1.

Table A1. Alloy composition [wt%] table of steels registered in NRIM atlas 1.

Material id	C	Si	Mn	Cu	Ni	Cr	Mo	V	N	Nb
2	0.090	0.370	1.340	0.110	0.020	0.000	0.010	0.060	0.0000	0.0000
3	0.160	0.410	1.220	0.080	0.020	0.000	0.000	0.000	0.0000	0.0000
4	0.170	0.380	1.310	0.110	0.040	0.000	0.010	0.040	0.0000	0.0000
5	0.160	0.240	0.830	0.000	0.030	0.040	0.000	0.000	0.0000	0.0000
7	0.130	0.400	0.830	0.240	0.950	0.480	0.500	0.000	0.0000	0.0000
8	0.150	0.330	1.030	0.250	0.800	0.380	0.440	0.000	0.0000	0.0000
9	0.150	0.350	1.060	0.250	0.810	0.430	0.400	0.000	0.0000	0.0000
11	0.110	0.380	0.990	0.120	0.860	0.540	0.300	0.000	0.0000	0.0000
12	0.150	0.250	1.100	0.240	0.650	0.110	0.210	0.000	0.0000	0.0000
13	0.150	0.450	1.270	0.210	0.070	0.050	0.020	0.000	0.0000	0.0000
14	0.130	0.480	1.370	0.000	0.000	0.220	0.000	0.130	0.0000	0.0000
15	0.150	0.450	1.330	0.000	0.000	0.290	0.000	0.140	0.0000	0.0000
16	0.110	0.370	1.340	0.000	0.470	0.270	0.000	0.100	0.0000	0.0000
17	0.140	0.450	1.220	0.000	0.480	0.320	0.000	0.120	0.0000	0.0000
18	0.160	0.460	1.350	0.150	0.000	0.000	0.000	0.000	0.0000	0.0000
19	0.070	0.200	0.750	0.210	0.430	0.510	0.110	0.080	0.0000	0.0000
20	0.070	0.290	0.370	0.120	3.120	1.280	0.280	0.000	0.0000	0.0000
21	0.140	0.160	0.750	0.150	1.910	0.630	0.470	0.000	0.0000	0.0000
22	0.110	0.310	0.490	0.000	2.030	1.250	0.370	0.000	0.0000	0.0000
24	0.130	0.400	0.970	0.130	0.520	0.550	0.280	0.050	0.0000	0.0000
25	0.150	0.270	0.400	0.160	2.490	1.190	0.260	0.000	0.0000	0.0000
26	0.090	0.350	0.380	0.000	2.460	1.180	0.290	0.000	0.0000	0.0000
27	0.100	0.190	0.410	0.000	2.500	1.010	0.290	0.000	0.0000	0.0000
28	0.220	0.120	1.080	0.000	0.000	0.000	0.000	0.000	0.0000	0.0000
29	0.090	0.240	1.150	0.000	0.000	0.000	0.000	0.000	0.0000	0.0000
30	0.090	0.210	0.400	0.000	2.460	1.000	0.270	0.000	0.0000	0.0000
31	0.130	0.250	0.350	0.000	2.500	1.170	0.270	0.000	0.0000	0.0000
33	0.150	0.530	1.200	0.000	0.090	0.030	0.000	0.000	0.0000	0.0000
34	0.110	0.480	1.200	0.000	0.080	0.050	0.000	0.000	0.0000	0.0000
35	0.180	0.470	1.400	0.000	0.040	0.050	0.000	0.000	0.0000	0.0000
37	0.130	0.550	0.540	0.000	2.540	1.230	0.500	0.000	0.0000	0.0000
38	0.090	0.200	0.400	0.080	3.410	1.020	0.270	0.000	0.0000	0.0000
39	0.150	0.340	0.380	0.090	2.920	0.740	0.530	0.000	0.0000	0.0000
40	0.190	0.350	0.550	0.000	2.680	1.210	0.540	0.000	0.0000	0.0000
41	0.220	0.500	0.980	0.280	3.000	0.510	0.500	0.010	0.0000	0.0000
44	0.110	0.340	1.210	0.000	0.450	0.200	0.150	0.000	0.0000	0.0000
45	0.120	0.340	0.800	0.000	1.200	0.440	0.320	0.000	0.0000	0.0000
46	0.180	0.540	1.270	0.000	0.120	0.140	0.000	0.000	0.0000	0.0000
47	0.160	0.280	0.360	0.000	2.250	1.200	0.420	0.000	0.0000	0.0000
48	0.100	0.230	0.600	0.000	2.650	0.470	0.450	0.000	0.0000	0.0000
49	0.140	0.320	1.320	0.000	0.000	0.000	0.000	0.003	0.0000	0.0000
51	0.120	0.230	0.360	0.000	0.000	1.940	1.320	0.000	0.0000	0.0000
52	0.400	0.880	0.360	0.000	0.120	4.750	1.240	0.560	0.0000	0.0000
53	0.180	0.470	1.400	0.170	0.040	0.050	0.000	0.000	0.0000	0.0000
54	0.130	0.410	1.080	0.160	0.020	0.020	0.000	0.000	0.0000	0.0000
55	0.160	0.450	1.180	0.210	0.020	0.020	0.000	0.000	0.0000	0.0000
56	0.100	0.010	0.410	0.180	0.020	0.030	0.000	0.000	0.0000	0.0000
57	0.110	0.020	0.610	0.150	0.020	0.030	0.000	0.000	0.0000	0.0000
58	0.140	0.230	0.650	0.160	0.020	0.020	0.000	0.000	0.0000	0.0000
59	0.140	0.090	0.960	0.180	0.060	0.070	0.000	0.000	0.0000	0.0000
60	0.130	0.230	1.180	0.130	0.040	0.040	0.000	0.000	0.0000	0.0000
61	0.150	0.420	1.210	0.140	0.060	0.040	0.000	0.000	0.0000	0.0000
62	0.140	0.530	1.120	0.060	0.060	0.040	0.000	0.000	0.0000	0.0000
63	0.180	0.320	1.200	0.070	0.650	0.220	0.130	0.130	0.0000	0.0000
64	0.110	0.420	1.120	0.070	0.470	0.270	0.160	0.130	0.0000	0.0000
66	0.170	0.340	1.310	0.000	0.000	0.000	0.000	0.000	0.0000	0.0000
68	0.240	1.490	0.970	0.000	1.860	0.990	0.380	0.000	0.0000	0.0000
69	0.250	1.760	1.320	0.000	1.860	0.100	0.360	0.000	0.0000	0.0000
70	0.230	1.500	0.970	0.000	1.860	0.910	0.390	0.000	0.0000	0.0000
71	0.250	1.450	1.360	0.000	1.740	0.100	0.400	0.000	0.0000	0.0000
72	0.300	1.510	0.750	0.000	1.840	0.840	0.450	0.000	0.0000	0.0000
73	0.150	0.280	0.970	0.000	0.020	0.010	0.000	0.000	0.0000	0.0270
74	0.190	0.040	1.000	0.000	0.020	0.620	0.000	0.000	0.0000	0.0000
75	0.130	0.440	1.440	0.000	0.180	0.000	0.000	0.000	0.0000	0.0260
76	0.110	0.290	1.470	0.000	0.000	0.000	0.000	0.000	0.0000	0.0270
77	0.160	0.480	1.420	0.000	0.000	0.000	0.000	0.000	0.0000	0.0000
78	0.170	0.240	1.340	0.210	0.040	0.020	0.000	0.000	0.0000	0.0000
79	0.130	0.480	1.400	0.150	0.030	0.040	0.000	0.000	0.0000	0.0000
80	0.110	0.000	0.460	0.000	0.000	0.000	0.000	0.000	0.0000	0.0000
81	0.110	0.220	0.460	0.000	0.000	0.000	0.000	0.000	0.0000	0.0000

(*Continued*)

Sci. Technol. Adv. Mater. Meth. 2 (2022) 414

S. MINAMOTO et al.

Table A1. (Continued).

Material id	C	Si	Mn	Cu	Ni	Cr	Mo	V	N	Nb
82	0.110	0.560	0.470	0.000	0.000	0.000	0.000	0.000	0.0000	0.0000
83	0.120	1.100	0.430	0.000	0.000	0.000	0.000	0.000	0.0000	0.0000
84	0.120	1.640	0.400	0.000	0.000	0.000	0.000	0.000	0.0000	0.0000
85	0.110	0.210	0.000	0.000	0.000	0.000	0.000	0.000	0.0000	0.0000
86	0.130	0.450	1.080	0.000	0.050	0.320	0.000	0.150	0.0000	0.0000
87	0.110	0.210	1.060	0.000	0.000	0.000	0.000	0.000	0.0000	0.0000
88	0.120	0.210	2.050	0.000	0.000	0.000	0.000	0.000	0.0000	0.0000
89	0.110	0.230	0.430	0.000	0.000	0.000	0.960	0.000	0.0000	0.0000
90	0.080	0.000	0.000	0.000	0.000	0.000	0.000	0.000	0.0000	0.0000
91	0.150	0.000	0.000	0.000	0.000	0.000	0.000	0.000	0.0000	0.0000
92	0.300	0.000	0.000	0.000	0.000	0.000	0.000	0.000	0.0000	0.0000
93	0.380	0.000	0.000	0.000	0.000	0.000	0.000	0.000	0.0000	0.0000
97	0.120	0.160	0.450	0.000	0.000	0.000	0.480	0.000	0.0000	0.0000
98	0.110	0.220	0.370	0.000	0.000	0.000	1.660	0.000	0.0000	0.0000
99	0.110	0.000	0.000	0.000	1.070	0.000	0.000	0.000	0.0000	0.0000
100	0.140	0.000	0.000	0.000	2.430	0.000	0.000	0.000	0.0000	0.0000
101	0.110	0.000	0.000	0.000	3.490	0.000	0.000	0.000	0.0000	0.0000
102	0.160	0.000	0.000	0.000	5.060	0.000	0.000	0.000	0.0000	0.0000
103	0.140	0.000	0.000	0.000	7.020	0.000	0.000	0.000	0.0000	0.0000
104	0.100	0.000	0.000	0.000	9.110	0.000	0.000	0.000	0.0000	0.0000
105	0.110	0.220	0.350	0.000	0.000	0.470	0.000	0.000	0.0000	0.0000
106	0.100	0.230	0.350	0.000	0.000	1.000	0.000	0.000	0.0000	0.0000
107	0.100	0.230	0.350	0.000	0.000	1.970	0.000	0.000	0.0000	0.0000
108	0.090	0.220	0.370	0.000	0.000	3.860	0.000	0.000	0.0000	0.0000
109	0.080	0.250	0.490	0.000	3.480	0.620	0.300	0.000	0.0000	0.0000
110	0.190	0.230	1.250	0.000	0.660	0.070	0.540	0.000	0.0000	0.0000
111	0.150	0.400	1.190	0.000	0.090	0.000	0.000	0.000	0.0000	0.0000
112	0.190	0.410	1.170	0.000	0.000	0.060	0.000	0.000	0.0000	0.0000
113	0.180	0.400	1.160	0.000	0.000	0.080	0.000	0.120	0.0000	0.0000
114	0.130	0.460	1.220	0.000	0.080	0.000	0.000	0.010	0.0000	0.0000
115	0.120	0.450	1.170	0.000	0.000	0.320	0.250	0.140	0.0000	0.0000
116	0.150	0.280	1.340	0.000	1.150	0.020	0.310	0.000	0.0000	0.0000
117	0.150	0.350	1.280	0.000	0.470	0.080	0.210	0.100	0.0000	0.0000
118	0.150	0.340	0.920	0.000	0.290	0.100	0.510	0.000	0.0000	0.0000
119	0.070	0.500	1.490	0.000	0.500	0.120	0.300	0.000	0.0000	0.0000
120	0.140	0.260	1.280	0.000	0.860	0.500	0.460	0.000	0.0000	0.0000
121	0.200	0.210	1.260	0.000	0.800	0.300	0.550	0.000	0.0000	0.0000
122	0.150	0.260	1.020	0.000	0.600	0.100	0.370	0.080	0.0000	0.0000
123	0.150	0.290	1.200	0.000	0.710	0.360	0.510	0.010	0.0000	0.0000
124	0.130	0.380	1.160	0.000	0.560	0.270	0.000	0.120	0.0000	0.0000
127	0.130	0.350	0.910	0.000	0.810	0.460	0.330	0.000	0.0000	0.0000
128	0.110	0.380	1.060	0.000	0.000	0.440	0.480	0.120	0.0000	0.0000
129	0.140	0.230	1.020	0.000	0.500	0.550	0.470	0.060	0.0000	0.0000
130	0.140	0.220	1.400	0.000	0.760	0.000	0.550	0.000	0.0000	0.0000
131	0.140	0.350	0.910	0.000	1.360	0.490	0.470	0.020	0.0000	0.0000
132	0.100	0.200	0.420	0.000	2.940	1.450	0.400	0.000	0.0000	0.0000
133	0.100	0.180	0.650	0.000	3.580	0.350	0.440	0.000	0.0000	0.0000
134	0.130	0.320	0.450	0.000	2.510	1.590	0.440	0.000	0.0000	0.0000
135	0.110	0.280	0.970	0.000	3.470	1.500	0.380	0.000	0.0000	0.0000
137	0.160	0.450	1.120	0.000	0.040	0.060	0.020	0.011	0.0000	0.0000
138	0.160	0.430	1.310	0.000	0.040	0.060	0.020	0.017	0.0000	0.0000
139	0.160	0.510	1.100	0.000	0.040	0.060	0.010	0.011	0.0000	0.0000
140	0.210	0.460	1.180	0.000	0.100	0.120	0.020	0.017	0.0000	0.0000
141	0.200	0.400	1.120	0.000	0.050	0.090	0.010	0.009	0.0000	0.0000
142	0.210	0.480	1.190	0.000	0.060	0.050	0.010	0.009	0.0000	0.0000
143	0.110	0.170	1.240	0.000	0.210	0.180	0.150	0.000	0.0000	0.0000
144	0.100	0.390	0.970	0.000	0.140	0.500	0.330	0.000	0.0000	0.0000
147	0.070	0.240	0.420	0.000	9.330	0.000	0.000	0.000	0.0000	0.0000
148	0.070	0.490	1.490	0.000	0.570	0.120	0.280	0.000	0.0000	0.0000
149	0.080	0.170	0.610	0.000	2.550	0.700	0.430	0.000	0.0000	0.0000
150	0.120	0.310	0.530	0.000	3.550	0.520	0.300	0.000	0.0000	0.0000
151	0.140	0.350	0.520	0.000	3.060	0.950	0.310	0.060	0.0000	0.0000
152	0.090	0.290	0.530	0.000	3.530	0.900	0.360	0.000	0.0000	0.0000
153	0.110	0.250	0.620	0.000	3.400	1.430	0.420	0.000	0.0000	0.0000
154	0.080	0.400	0.610	0.000	3.710	1.460	0.570	0.000	0.0000	0.0000
157	0.100	0.350	0.780	0.000	1.290	0.440	0.290	0.000	0.0000	0.0000
159	0.150	0.250	0.850	0.000	0.860	0.520	0.420	0.055	0.0000	0.0000
160	0.160	0.230	0.820	0.000	2.000	0.780	0.490	0.070	0.0000	0.0000
162	0.160	0.230	1.160	0.000	1.540	0.500	0.420	0.026	0.0000	0.0560
163	0.100	0.280	0.570	0.000	2.540	0.790	0.450	0.000	0.0000	0.0000
164	0.130	0.380	0.890	0.000	3.340	0.580	0.360	0.090	0.0000	0.0000
165	0.110	0.320	0.460	0.000	3.380	0.980	0.290	0.000	0.0000	0.0000
166	0.140	0.290	0.870	0.000	0.810	0.560	0.460	0.090	0.0000	0.0000
167	0.150	0.350	1.030	0.000	0.800	0.380	0.440	0.000	0.0000	0.0000
170	0.110	0.230	0.420	0.000	0.000	0.000	0.000	0.000	0.0000	0.0950
171	0.170	0.220	0.400	0.000	0.000	0.000	0.000	0.000	0.0000	0.1100
172	0.110	0.230	0.410	0.000	0.000	0.000	0.000	0.100	0.0000	0.0000

(*Continued*)

Sci. Technol. Adv. Mater. Meth. 2 (2022) 415

S. MINAMOTO et al.

Table A1. (Continued).

Material id	C	Si	Mn	Cu	Ni	Cr	Mo	V	N	Nb
174	0.110	0.230	0.400	0.420	0.000	0.000	0.000	0.000	0.0000	0.0000
175	0.050	0.200	1.520	0.000	0.400	0.160	0.190	0.000	0.0000	0.0420
176	0.040	0.300	1.500	0.000	0.010	0.020	0.010	0.041	0.0000	0.0350
177	0.090	0.280	0.830	0.000	2.650	0.000	0.010	0.000	0.0000	0.0000
178	0.090	0.220	1.350	0.000	0.000	0.350	0.240	0.000	0.0000	0.0080
179	0.120	0.250	0.480	0.040	0.040	0.640	0.510	0.000	0.0130	0.0000
180	0.120	0.360	0.520	0.040	0.090	0.970	0.610	0.000	0.0066	0.0000
181	0.120	0.650	0.550	0.040	0.060	1.420	0.540	0.000	0.0049	0.0000
182	0.120	0.260	0.480	0.080	0.080	2.000	0.960	0.080	0.0096	0.0000
183	0.120	0.360	0.450	0.050	0.050	4.610	0.500	0.000	0.0150	0.0000
184	0.120	0.330	1.370	0.000	0.190	0.030	0.010	0.080	0.0000	0.0000
185	0.070	0.250	0.670	0.000	3.960	0.620	0.460	0.060	0.0000	0.0000
186	0.070	0.280	1.250	0.000	0.000	0.000	0.000	0.000	0.0000	0.0000
187	0.100	0.240	0.600	0.000	3.510	0.000	0.000	0.000	0.0000	0.0000
188	0.060	0.240	1.120	0.000	5.750	0.580	0.190	0.000	0.0000	0.0000
189	0.180	0.380	1.340	0.000	0.000	0.000	0.000	0.000	0.0000	0.0000
190	0.140	0.250	0.580	0.000	0.000	0.000	0.000	0.000	0.0000	0.0000
191	0.130	0.250	0.520	0.000	0.000	2.210	1.020	0.000	0.0000	0.0000
192	0.120	0.280	0.590	0.000	0.000	1.080	0.310	0.230	0.0000	0.0000
193	0.088	0.270	0.490	0.000	0.000	0.770	0.470	0.000	0.0000	0.0000
195	0.160	0.360	0.580	0.000	0.000	1.050	0.420	0.000	0.0000	0.0000